Morphology and Properties of PET/PA-6/SiO_2 Ternary Composites

Cheng Qu, Hong Yang, Dong Liang, Wen Cao, Qiang Fu

Department of Polymer Science and Materials, State Key Laboratory of Polymer Materials Engineering, Sichuan University, Chengdu 610065, China

Received 13 April 2006; accepted 22 October 2006
DOI 10.1002/app.25690
Published online in Wiley InterScience (www.interscience.wiley.com).

ABSTRACT: A kind of hydrophilic nano-SiO_2 was applied to poly(ethylene terephthalate)/polyamide-6 (PA-6) blends. Melt-blended composites were prepared at various component ratios and different nano-SiO_2 levels. Mechanical, morphological, dynamic mechanical, and thermal tests were carried out to characterize the properties, morphology, and compatibilization of the composites. Increased impact strength, tensile strength, and modulus were observed by adding nano-SiO_2 particles in the blends. The nano-SiO_2 particles were found to be preferentially dispersed in PA-6, resulting in an increase of glass transition temperature and crystallization of PA-6. The mechanism of morphology and properties changes was discussed based on the selective dispersion of nano-SiO_2 particles in the blends. © 2007 Wiley Periodicals, Inc. J Appl Polym Sci 104: 2288–2296, 2007

Key words: polyesters; polyamides; silicas; selective dispersion

INTRODUCTION

Polymer blends are important in industry, since they can be obtained with desirable properties through relatively simple and low-cost processing. poly(ethylene terephthalate) (PET)/polyamide-6 (PA-6) could be such a promising blending material for engineering and food-packaging, if it combines good comprehensive properties of PET with the toughness and high barrier of PA-6. However, PET/PA-6 blend has rarely been used until recently, because of the poor compatibility between PET and PA-6, which makes the properties of the blend inferior to those of neat PET or PA-6.

So the property modification and morphology control of PET/PA-6 blends become attractive. A lot of work has been done in this direction.[1–18] Some researchers designed and developed various compatibilizers, while others focused on promoting the interaction of PET and PA-6. Samios and Kalfoglou[1] applied an acrylic-modified polyolefin type ionomer to PET/PA-6 composites as compatibilizer. They prepared melt-mixed blends with various amounts of the ionomer, and found that compatibilization was attained when adding more than 10 wt % ionomer. Huang et al.[2] incorporated a low-molecular-weight bisphenol-A epoxy resin as reactive compatibilizer with PET and PA-6. When the content of epoxy resin was 5 wt %, the notched impact strength and flexural strength of the PET/PA-6 composites were significantly improved. IR results indicated that grafting reaction and crosslinking reaction occurred during melt blending. Fakirov et al.[3,4] studied binary blends of PET and PA-6, and found that additional condensation and exchange reactions took place at the interfaces, resulting in the formation of PET-PA-6 block copolymers. Serhatkulu et al.[5] examined the thermomechanical behavior of PET/PA-6 blends by means of dynamic mechanical analysis (DMA). They attributed the increase of compatibility to transreactions producing compatibilizing layers at phase boundaries. Pillon and coworkers[6–9] utilized *p*-toluenesulfonic acid as a catalyst to promote the ester–amide interchange reaction during PET/PA-66 melt blending and improved impact and tensile strengths. Evstatiev et al.[10] investigated microfibrillar reinforced PET/PA-6 blends and concluded the occurrence of chemical interactions from the complete loss of crystallinity of the PA-6 component. Evstatiev et al.[11] also studied *in situ* fibrillar reinforced PET/PA-6/PA-66 blends in the presence of a catalyst. The differential scanning calorimetry (DSC) results suggested an *in situ* generation of copolymer, which improved the compatibility of the blend components. Retolaza et al.[12,13] obtained PET/PA-6 and PET/PA-66 blends by direct injection molding and they attributed the finely dispersed blending to the presence of reacted copolymers.

In recent years, there has been intense interest in the application of inorganic nanoparticles as property-modifiers for immiscible polymer blends. Ray

Correspondence to: Q. Fu (qiangfu@scu.edu.cn).
Contract grant sponsor: National Natural Science Foundation of China; contract grant numbers: 20404008, 50533050, 20490220.

et al.[19] investigated the role of organically modified layered silicate for PS/PP immiscible composites. XRD and TEM observations showed that silicate layers were located at the interface between the two polymers, and it resulted in a decrease in interfacial tension and particle size and in a remarkable increase in mechanical properties. Then, Ray and Bousmina[20] studied the property-modification action of organically modified montmorillonite for PC/PMMA composites and indicated that the key factor for modification efficiency of the organoclay was the initial interlayer spacing. Río et al.[21] reported that partial polymer compatibilization and modification of the isothermal crystallization took place in PVDF/PA composites after adding carbon black, and they concluded it as a consequence of an improvement in component adhesion. Our group prepared PP/EPDM/SiO_2 ternary composites and found a unique structure with the majority of EPDM particles surrounded by SiO_2 particles, which resulted in a dramatic increase of Izod impact strength.[22] Besides, some theories or models have been proposed to explain how the inorganic nanoparticles induced change of phase morphology in polymer blends.[23–34]

In the present study, the effect of nano-SiO_2 on the properties and morphology of PET/PA-6 was estimated in the ternary composites prepared at various component ratios and different nano-SiO_2 levels. The structure-and-property relationship of as-prepared composites has been established according to the results of mechanical, DMA, morphological, and thermal measurements. On the basis of the selective dispersion of nano-SiO_2 particles in the blends, the mechanism of morphology and properties changes was discussed.

EXPERIMENTAL

Materials

PET was bottle grade obtained from Chenguang Research Institute of Chemical Industry, with intrinsic viscosity of 0.80 ± 0.02 dL/g, density of 1.41 g/cm^3, and melting point of (248 ± 1)°C. PA-6 was purchased from BASF chemical company with commercial trademark Unreinforced Ultramid B3S, with a density of 1.13 g/cm^3 and melting point of 220°C. Nano-SiO_2 used in our study was HL-150 hydrophilic SiO_2 from Guangzhou GBS High Tech and Industry Co., the particle size was 15–20 nm and $S_{(BET)}$ was 150 ± 10 m^2/g.

Specimen preparation

Composites of different compositions were prepared using a twin-screw extruder (TSSJ-25/32). Barrel temperatures were set at 190–260°C and the screw speed was 120 rpm. The filaments obtained upon extrusion were immediately quenched in water, and then cut into pellets by a pelletizer.

The pellets were injection molded into standard specimen (GB104IIdumbbell shaped bars, 150 × 10 × 4.2 mm^3) by using an injection molding machine (PS40E5ASE). The temperature was chosen at 280–255°C from die to hopper.

Prior to extrusion and injection, the composites were dried in a vacuum oven at 90°C for 24 h.

Mechanical testing

Tensile tests were conducted on dumbbell shaped specimens using an AG-10TA tensile testing machine at (23 ± 2)°C. Test speed was first set at 5 mm/min and then kept at 50 mm/min. For impact strength tests, the notched specimens were tested with an I200XJU-2.75 impact tester at room temperature. Each result was averaged from the impact strengths of at least five specimens.

Dynamic mechanical analysis

The dynamic mechanical analysis (DMA) was carried out using a TA Instruments Q800 DMA. All the samples were measured in a dual cantilever mode over the temperature range of −20 to 180°C at a heating rate of 3°C/min and at a frequency of 1 Hz. Specimen dimensions were 40 × 10 × 4.2 mm^3.

Scanning electron microscopy

Scanning electron microscopy (SEM) was carried out on surfaces of cryo-fractured or tensile fractured specimens after gold coating. A JEOL JSM-5900LV SEM instrument was used at an accelerating voltage of 20 kV. The cryo-fractured specimens were pretreated by selective etching of PA-6 phase in formic acid for 5 min.

Differential scanning calorimetry

Investigation of thermal behaviors was accomplished with a Perkin–Elmer DSC, Model Pyris 1. The samples were kept at 290°C for 5 min to delete the thermal history. Then, they were cooled down to room temperature at a rate of 10°C/min to obtain the crystallization curves and were heated again to 290°C at a rate of 10°C/min to obtain the melting curves.

Fourier transform infrared spectroscopy

Fourier transmission infrared spectra (FTIR) were obtained by using a Nicolet 560 MAGNA IR spectrometer. The films were obtained by compressing the composites at 400 kg/cm^2 with a laboratory press.

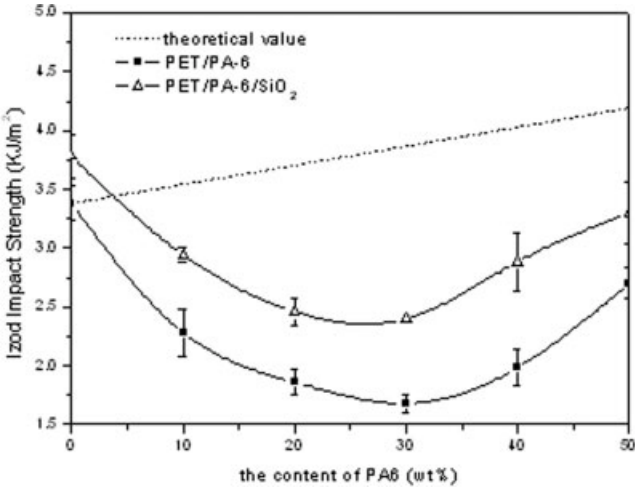

Figure 1 Izod impact strength of PET/PA-6/nano-SiO_2 system.

RESULTS

Mechanical properties

Figure 1 shows the impact strength of PET/PA-6 binary blends and PET/PA-6/nano-SiO_2 ternary composites as a function of PA-6 content. One observes a decrease of impact strength PET/PA-6 binary blends by adding PA-6 at lower content (less than 30 wt %), due to the poor compatibility between PET and PA-6. The increase of impact strength is seen as PA-6 content is above 30 wt %, and this could be understood as due to the change of phase morphology from droplets to cocontinuous structure. After the addition of nano-SiO_2 (1 wt %), the toughness of the composite is obviously enhanced in the whole composition range investigated. However, the impact values are still lower than the theoretical ones that could be predicted from ''mixing rule'' of polymer blending.

Figures 2 and 3 summarize the tensile properties of the materials. For PET/PA-6 binary blends, the tensile strength is lower than the theoretical value. For PET/PA-6/nano-SiO_2 ternary system, the addition of nano-SiO_2 increases the tensile strength of the composite to the theoretical value. Besides, the tensile modulus is also enhanced, and this can be easily attributed to the rigidity of nano-SiO_2 particles.

Morphology

To observe the morphological change of PET/PA-6 blends resulted from the addition of nano-SiO_2 and the dispersion of nano-SiO_2 particles, SEM was carried out on the surface of cryo-fractured and etched specimens. For comprehensive analysis, samples with a variety of PET/PA-6 ratios, 90/10, 70/30, 50/50, respectively, were chosen.

Figure 4 shows the SEM observation of the 90/10 samples with different amount of nano-SiO_2. PA-6 phase was etched by formic acid, leaving cavities in PET matrix. For the blends without nano-SiO_2, PA-6 is dispersed in PET matrix as spherical particles with uniform shape and size. The interface between the spheres and matrix is smooth, which indicates the poor compatibility of PET and PA-6. As for the blends with 1 wt % nano-SiO_2, one observes some morphological changes. The cavities become larger and are not in spherical shape, and the apparent volume of PA-6 seems to be increased. Most of nano-SiO_2 is observed in the cavities and on the interfaces. Some nano-SiO_2 particles are found in PET matrix and the adhesion between nano-SiO_2 and the surface of PET seems weak. The size of nano-SiO_2 agglomerates observed is ~0.1 μm, much bigger than a single nano-SiO_2 particle (15–20 nm). It means nano-SiO_2 particles are easy to aggregate and dispersed poorly in PET/

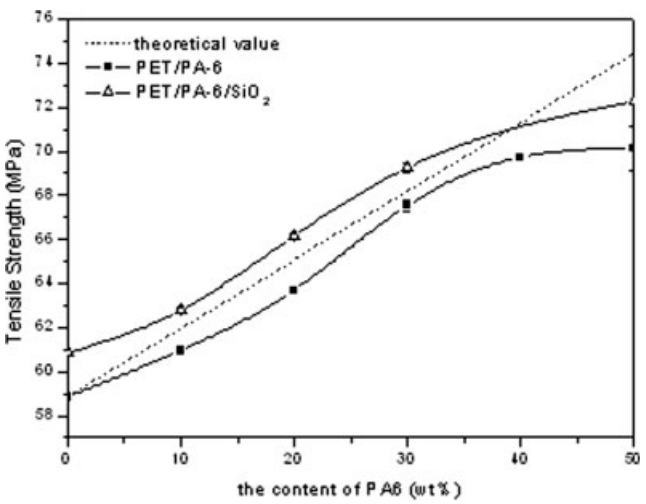

Figure 2 Tensile strength of PET/PA-6/nano-SiO_2 system.

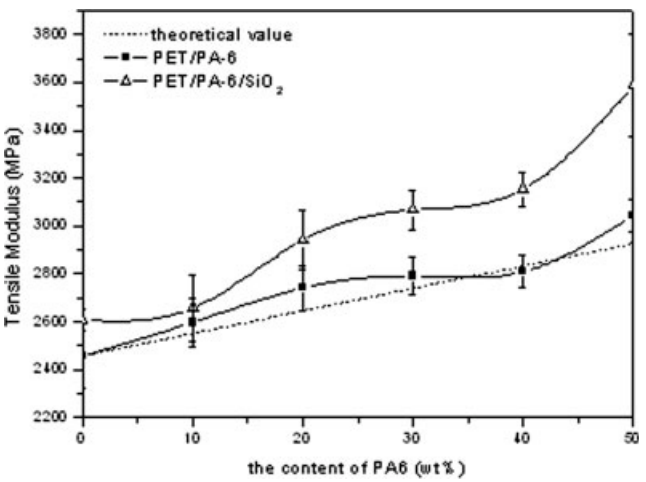

Figure 3 Tensile modulus of PET/PA-6/nano-SiO_2 system.

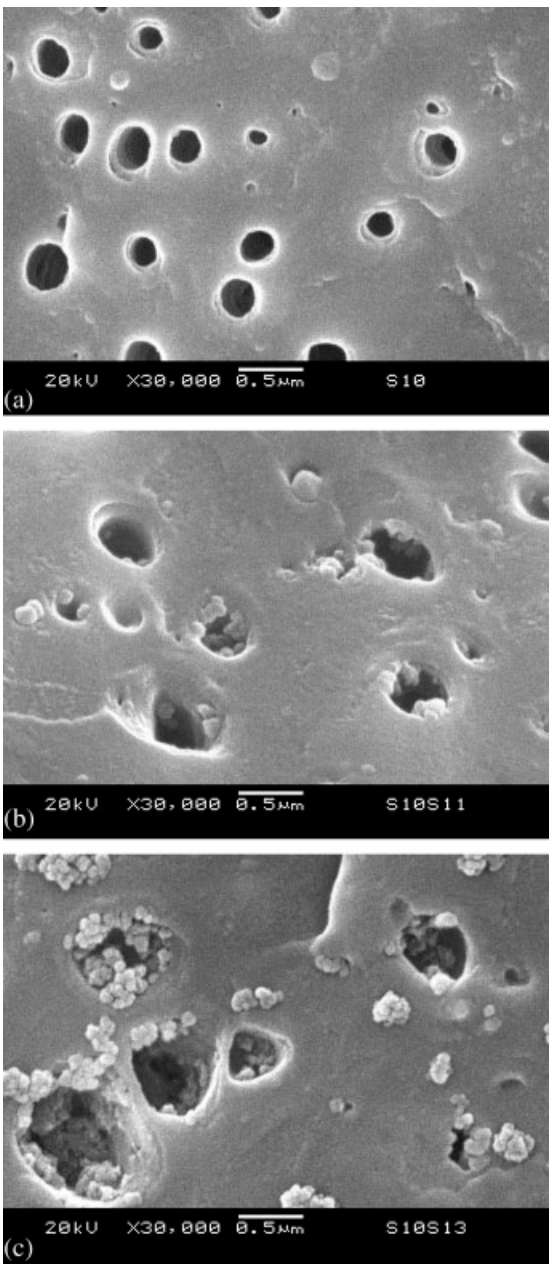

Figure 4 SEM images of cryo-fractured PET/PA-6/nano-SiO_2 composites: (a) 90/10/0; (b) 90/10/1; (c) 90/10/3.

PA-6 blends as agglomerates. The more nano-SiO_2 is added, the more serious the aggregation.

The morphology of the 70/30 samples is shown in Figure 5. For the blends without nano-SiO_2, the morphology changes little with the increase of PA-6 content [compared with Fig. 4(a)]. PA-6 is dispersed in a spherical shape, the size of PA-6 cavities and the smoothness of the interface keeps the same. After the addition of 1 wt % nano-SiO_2, the size of cavities increases a lot, and the cavities with nano-SiO_2 are larger than those with no nano-SiO_2. In the elliptical cavities, nano-SiO_2 agglomerates aggregate to be big lumps. Also, no nano-SiO_2 particles are found in the PET matrix.

The morphology of 50/50 samples is also observed, as shown in Figure 6. In the binary blends [Fig. 6(a)], a mass of columns, parallel to the flow direction, are found. Considering that PA-6 phase was etched, the columns are PET. Most of the columns with uniform diameters are dispersed symmetrically in PA-6 matrix. In this case instead of the droplets, a cocontinuous morphology is formed. A change of morphology is seen with the addition of 1 wt % nano-SiO_2 [Fig. 6(b)]. The columns are inequable in size and shape. In other words, the phase structure becomes unsteady. Again, no nano-SiO_2 particles or agglomerates are found in PET [Fig. 6(c)].

Dynamic mechanical property

DMA was applied to measure the compatibility of PET/PA-6 blends, and the temperature dependence of dynamic modulus for PET/PA-6 (1 : 1 by weight) blends at various nano-SiO_2 levels is shown in Figure 7. It is well established that the maximum of the tan δ curve is considered as the glass transition temperature of the material. Since the loss modulus E'' curve can provide better resolution than the tan δ

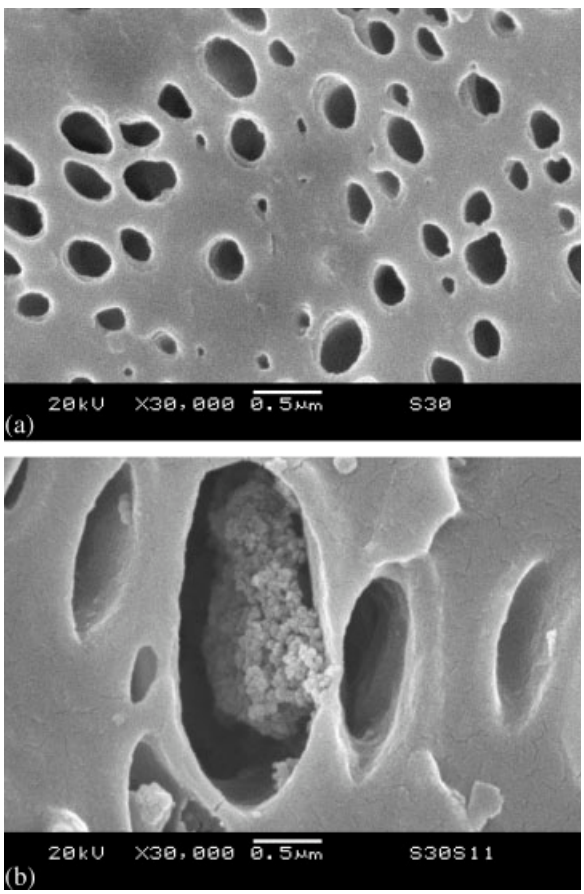

Figure 5 SEM images of cryo-fractured PET/PA-6/nano-SiO_2 composites: (a) 70/30/0 and (b) 70/30/1.

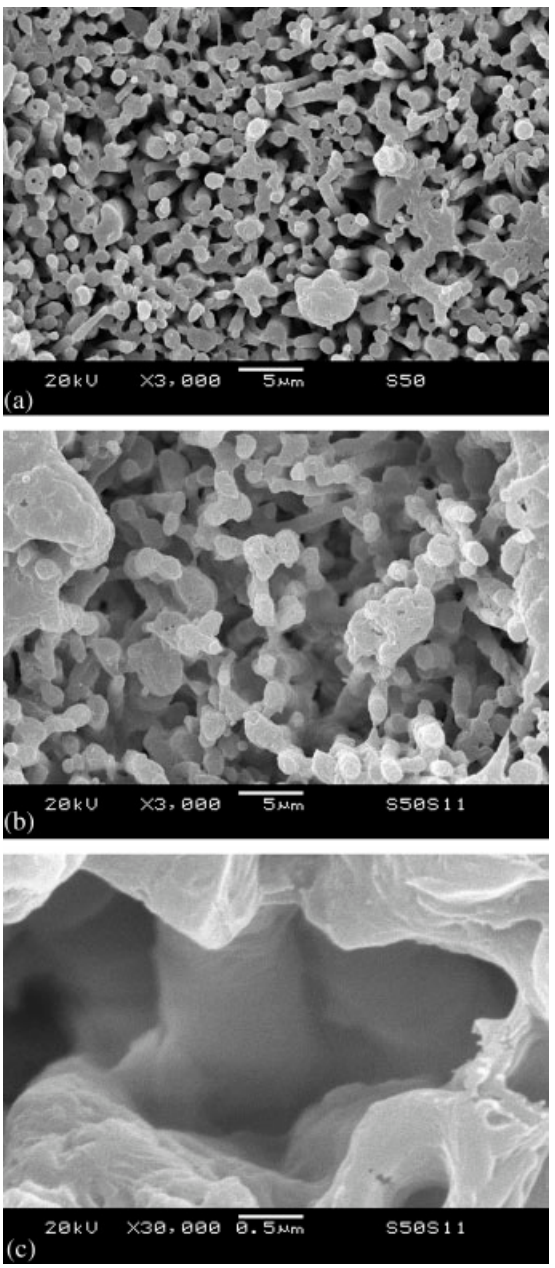

Figure 6 SEM images of cryo-fractured PET/PA-6/nano-SiO_2 composites: (a) 50/50/0; (b) 50/50/1 (×3000); (c) 50/50/1 (×30,000).

curve, it is used to evaluate the T_g of each component in the present work. The peak at ~80°C is the T_g of PET, while the peak at 25–35°C belongs to PA-6.[5]

It can be seen that the addition of nano-SiO_2 makes the T_g of PA-6 shift to higher temperature, and the increment becomes bigger with the increase of nano-SiO_2 content. In PET/PA-6 binary composite, the T_g of PA-6 is at ~28°C. After adding 1 wt % nano-SiO_2, it is changed to ~33°C. When the content of nano-SiO_2 is 5 wt %, it shifts to ~39°C. This can be attributed to the influence of nano-SiO_2. Because of the strong interaction between PA-6 molecular chains and surface of nano-SiO_2, as well as the volume effect of nano-SiO_2 rigid particles, the mobility of PA-6 chains is restricted, resulting in the increase of T_g. Meanwhile, the addition of nano-SiO_2 has no obvious effect on the T_g of PET, and only a shift of 1°C can be observed. Also, the addition of nano-SiO_2 changes the storage modulus E' of PET/PA-6 blends, i.e., it changes the stiffness of the system.

DISCUSSION

As shown earlier, the impact strength and tensile strength of PET/PA-6 blends are obviously enhanced by adding nano-SiO_2. However, the impact strengths are still lower than the theoretical ones. It means that nano-SiO_2 does not effectively modify the interface of the two components and make them compatible. In dynamic mechanical measurement, only the T_g of PA-6 obviously shifts after the addition of nano-SiO_2 reveals that the interfacial adhesion between PET and PA-6 is not effectively modified and preferential incorporation of nano-SiO_2 in PA-6 phase occurs in ternary composites. SEM results further demonstrate this. When nano-SiO_2 is added to the system, the size of PA-6 phase becomes larger, and most of nano-SiO_2 particles are dispersed in PA-6 phase, not on the interface between PET and PA-6 [Figs. 4(c) and 5(b)].

To further study the dispersion of nano-SiO_2, the crystallization behavior of PET/PA-6/nano-SiO_2 blends was investigated by DSC. In PET/PA-6 binary blends, an increasing amount of PA-6 raises the crys-

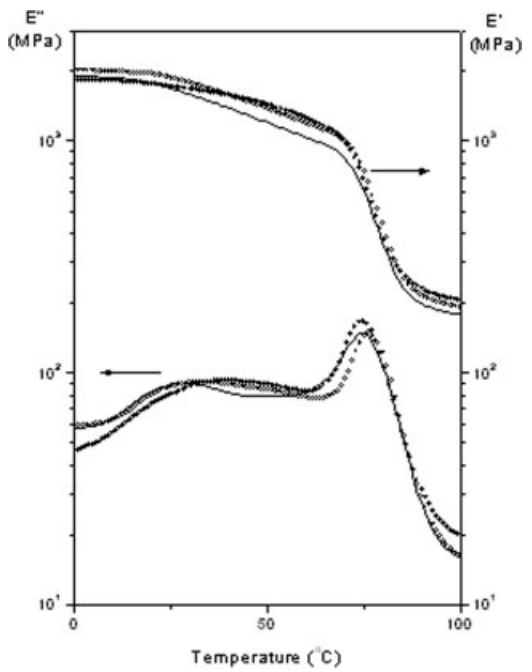

Figure 7 Temperature dependence of storage modulus E' and loss modulus E'' of PET/PA-6/nano-SiO_2 composites: (–) 50/50/0; (○) 50/50/1; (●) 50/50/5.

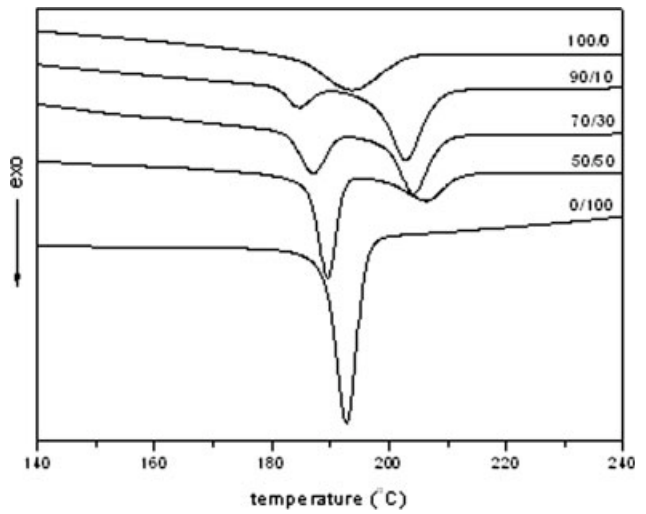

Figure 8 DSC crystallization curves of PET/PA-6 binary composites.

tallization temperature T_c of PET, i.e., PA-6 facilitates the crystallization of PET (Fig. 8). In PET/nano-SiO_2 composites, because of the nucleation effect of nano-SiO_2 particles, an increasing amount of nano-SiO_2 facilitates the crystallization of PET and thus shifts the crystallization peak to higher temperature (Fig. 9). However, when the ternary system contains both PA-6 and nano-SiO_2, which can facilitate the crystallization of PET separately, the crystallization of PET is restrained (Fig. 10). And when the content of PA-6 increases, the restraint of PET crystallization aggravates (shown in Table I). In the 90/10 blends, 1 wt % addition of nano-SiO_2 results in 0.5°C decrease of T_c; but in 50/50 composites, the reduction of T_c reaches 4.2°C. Besides, the crystallization behavior of PA-6 is influenced. When the content of PA-6 is low (10 wt %), the addition of nano-SiO_2 shift the T_c of PA-6 to lower temperature. But when the content of PA-6 increases to 50 wt %, a higher T_c of PA-6 is found after nano-SiO_2 is added. Considering the morphological observation [Fig. 5(b)], the preferential dispersion of nano-SiO_2 in PA-6 should account for the results.

To elucidate why nano-SiO_2 particles were selectively dispersed in PA6 phase, FTIR experiment was carried out. The IR spectra of PET/PA-6 and PET/PA-6/nano-SiO_2 composites are shown in Figure 11. The distinguished absorption bands of PET/PA-6 composite centered at 3428–3309 cm^{-1}, and 1638 cm^{-1} are corresponding to the motions of N—H stretching vibration and N—H bending vibration of PA-6. Because of hydrogen bonds between PA-6 molecules, part of absorption band (3428 cm^{-1}) corresponding to the motion of N—H stretching vibration shifts to lower frequency (3309 cm^{-1}). As to the PET/PA-6/nano-SiO_2 composite, the absorption band of N—H stretching vibration at 3309 cm^{-1} shifts to lower frequency (3304 cm^{-1}), with increased intensity; while the absorption band at 3428 cm^{-1} remains nearly the same frequency with decreased intensity. It can be explained that the hydrogen-bonded N—H groups of PA-6 increased after the addition of nano-SiO_2. Meanwhile, the absorption band of N—H bending vibration shifts to higher frequency (1641 cm^{-1}). The shifting of absorption bands of N—H stretching vibration and N—H bending vibration demonstrates that the hydrogen bonding of PET/PA-6 composite was enhanced with the addition of nano-SiO_2. It is

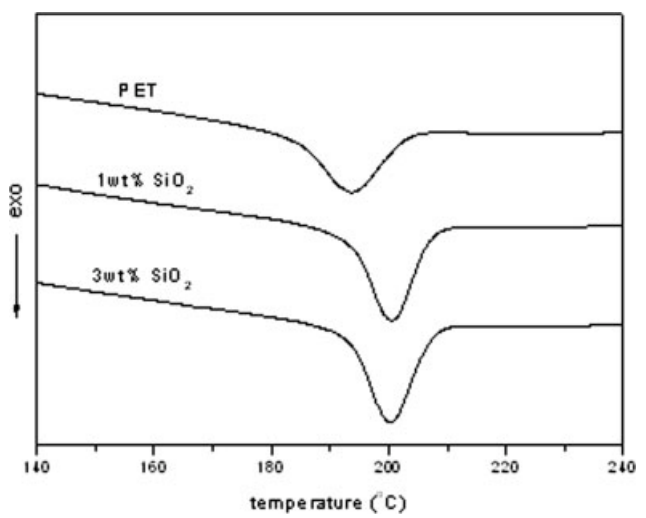

Figure 9 DSC crystallization curves of PET/nano-SiO_2 binary composites.

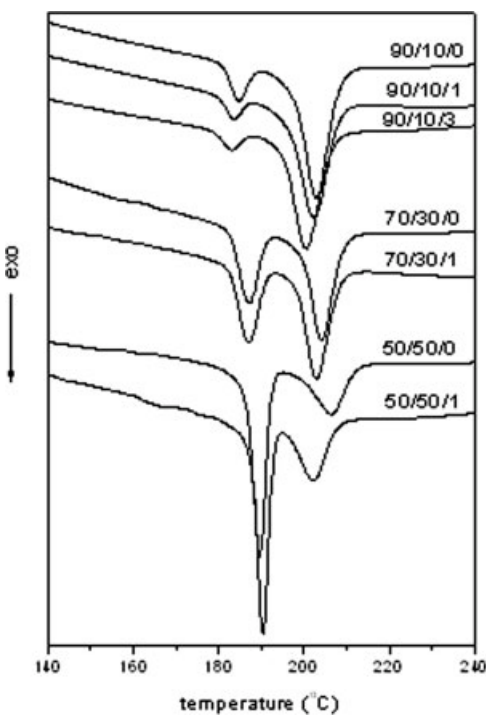

Figure 10 DSC crystallization curves of PET/PA-6/nano-SiO_2 ternary composites.

TABLE I
Thermal Properties of PET/PA-6/Nano-SiO_2 Composites

	T_c (°C)		ΔH_m (J/g)		X_c (%)	
Sample	PET	PA-6	PET	PA-6	PET	PA-6
100/0/0	193.695	\	28.587	\	23.432	\
0/100/0	\	192.783	\	60.489	\	31.836
100/0/1	200.528	\	29.702	\	24.346	\
100/0/3	200.240	\	29.629	\	24.286	\
90/10/0	202.867	184.511	28.073	4.714	25.567	24.811
90/10/1	202.370	183.503	26.902	1.227	24.501	6.458
90/10/3	200.501	182.969	24.253	1.219	22.088	6.416
70/30/0	204.129	187.108	21.061	10.390	24.662	18.228
70/30/1	202.961	186.946	19.249	12.582	22.540	22.074
50/50/0	206.449	189.443	13.408	24.587	21.980	25.881
50/50/1	202.282	190.277	12.796	25.135	20.977	26.458

possible that the *N*—H and C=O groups on polyamide chains form hydrogen bonds with the O—H groups on the surface of nano-SiO_2 particles[35] [Fig. 12(a)], and the O—H groups on the surface of nano-SiO_2 particles can also form hydrogen bonds with each other [Fig. 12(b)]. Except for those three absorption bands mentioned earlier, other ones remain the same frequencies after the addition of nano-SiO_2, which means PET did not participate in the formation of hydrogen bonds or react with nano-SiO_2. FTIR spectra reveal that the preferential incorporation of PA-6 and nano-SiO_2 can be attributed to the formation of hydrogen bonds between *N*—H and C=O groups on PA-6 chains and O—H groups on the surface of nano-SiO_2 particles.

To inspect the influence of nano-SiO_2 on the blends, SEM observation of tensile fractured surface was carried out (Fig. 13). Without nano-SiO_2, the interface between the two components is smooth and clear, and the drawn PET columns are distorted. This implies easy evulsions of PET columns during tensile tests. After the addition of 1 wt % nano-SiO_2, no distortion is observed to PET columns, and the gap between columns and matrix is negligible. PA-6/nano-SiO_2 phase has strong interaction with PET, and the enhanced interfacial adhesion worked when PET columns were drawn. This leads to a higher tensile strength (Fig. 2).

CONCLUSIONS

The effect of nano-SiO_2 on phase morphology and mechanical properties of PET/PA-6 blends was investigated in this study. After adding nano-SiO_2 particles into the blends, the impact strength, tensile strength, and modulus were obviously enhanced in the whole

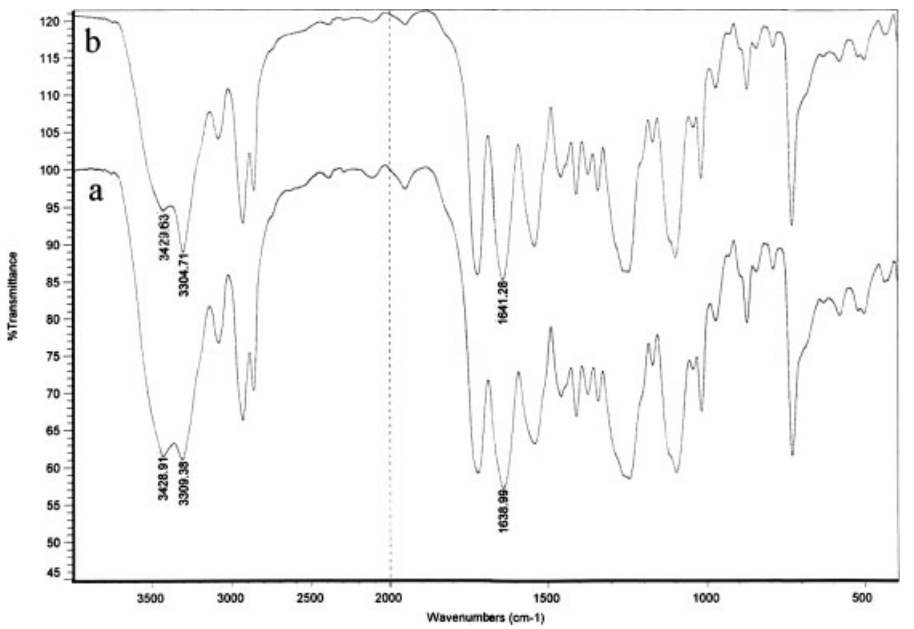

Figure 11 FTIR spectra of PET/PA-6 and PET/PA-6/nano-SiO_2 composites: (a) PET/PA-6 and (b) PET/PA-6/nano-SiO_2.

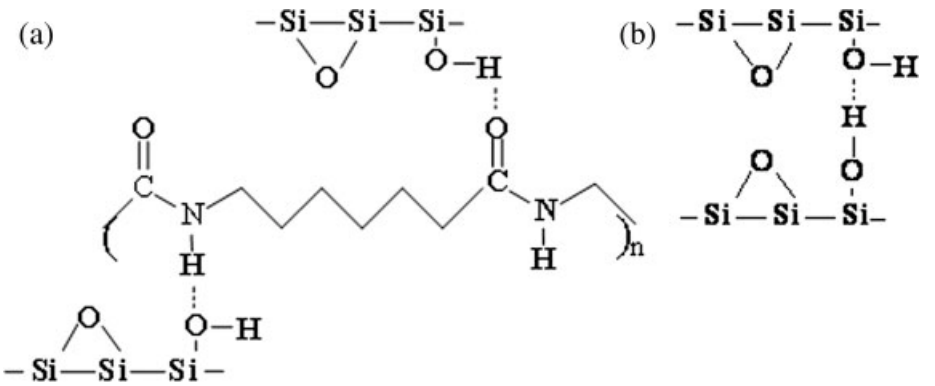

Figure 12 Schematics of the formation of hydrogen bonds: (a) O—H with *N*—H and C=O, (b) O—H with O—H.

composition range investigated. However, the impact values were still lower than the theoretical ones that could be predicted from ''mixing rule'' of polymer blending. The nano-SiO_2 particles were found to be preferentially dispersed in PA-6, and this leads to the increased size of PA-6 phase. Observation of tensile fractured surface revealed that the addition of nano-SiO_2 enhanced the interfacial adhesion between PET and PA-6. DMA results show that the addition of nano-SiO_2 makes the T_g of PA-6 shift to higher temperature, and the increment becomes bigger with the increase of nano-SiO_2 content. Meanwhile, the addition of nano-SiO_2 has no obvious effect on the T_g of PET. Only α-relaxation of PA-6 was confined by nano-SiO_2, revealing that nano-SiO_2 particles dispersed only in PA-6 phase, which was consisted well with the morphological observation. DSC data show that PA-6 and nano-SiO_2 particles can facilitate the crystallization of PET separately, but when the ternary system contains both PA-6 and nano-SiO_2, the crystallization of PET is restrained. It demonstrates the selective dispersion of nano-SiO_2 in PA-6. FTIR investigates the shifting of absorption bands of PET/PA-6 composite after the addition of nano-SiO_2 and attributes the selective dispersion of nano-SiO_2 to the formation of hydrogen bonds.

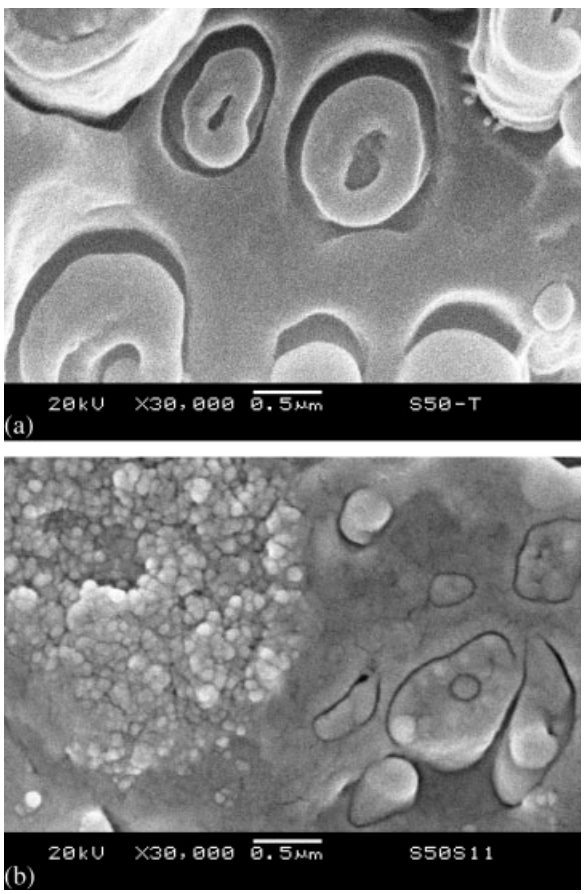

Figure 13 SEM images of tensile fractured PET/PA-6/nano-SiO_2 composites: (a) 50/50/0 and (b) 50/50/1.

It can be concluded that the phase morphology of PET/PA-6 could be prominently changed through adding nano-SiO_2 and thus results in increased mechanical properties, restricted molecular relaxations, and restrained crystallization.

This work is subsidized by the Special Funds for Major State Basic Research Projects of China (2003CB615600) and by Ministry of Education of China as a key project (104154).

References

1. Samios, C. K.; Kalfoglou, N. K. Polymer 1999, 40, 4811.
2. Huang, Y. Q.; Liu, Y. X.; Zhao, C. H. J Appl Polym Sci 1998, 69, 1505.
3. Fakirov, S.; Evstatiev, M.; Petrovich, S. Macromolecules 1993, 26, 5219.
4. Fakirov, S.; Evstatiev, M.; Schultz, J. M. Polymer 1993, 34, 4669.
5. Serhatkulu, T.; Erman, B.; Bahar, I.; Fakirov, S.; Evstatiev, M.; Sapundjieva, D. Polymer 1995, 36, 2371.
6. Pillon, L. Z.; Lara, J.; Pillon, D. W. Polym Eng Sci 1987, 27, 984.
7. Pillon, L. Z.; Utracki, L. A.; Pillon, D. W. Polym Eng Sci 1987, 27, 562.
8. Pillon, L. Z.; Utracki, L. A. Polym Eng Sci 1984, 24, 1300.
9. Pillon, L. Z.; Utracki, L. A. Polym Process Eng 1984, 4, 375.
10. Evstatiev, M.; Nicolov, N.; Fakirov, S. Polymer 1996, 37, 4455.

11. Evstatiev, M.; Schultz, J. M.; Fakirov, S.; Friedrich, K. Polym Eng Sci 2001, 41, 192.
12. Retolaza, A.; Eguiazabal, J. I.; Nazabal, J. J Appl Polym Sci 2005, 97, 564.
13. Retolaza, A.; Eguiazabal, J. I.; Nazabal, J. Polym Eng Sci 2004, 44, 1405.
14. Ellis, T. S. Polymer 1997, 38, 3837.
15. Krumova, M.; Fakirov, S.; Calleja, F. J. B.; Evstatiev, M. J Mater Sci 1998, 33, 2857.
16. Tjong, S. C.; Li, R. K. Y.; Xie, X. L. Polym J 2000, 32, 907.
17. Nagasawa, T.; Murata, Y.; Tadano, K.; Kawai, R.; Ikehara, K.; Yano, S. J Mater Sci 2000, 35, 3077.
18. Sapoundjieva, D.; Denchev, Z.; Evstatiev, M.; Fakirov, S.; Stribeck, N.; Stamm, M. J Mater Sci 1999, 34, 3063.
19. Ray, S. S.; Pouliota, S.; Bousminaa, M.; Utracki, L. A. Polymer 2004, 45, 8403.
20. Ray, S. S.; Bousmina, M. Macromol Rapid Commun 2005, 26, 450.
21. Río; Ojeda, M. C.; Acosta, J. L. Eur Polym J 2000, 36, 1687.
22. Yang, H.; Zhang, Q.; Guo, M.; Wang, C.; Du, R. N.; Fu, Q. Polymer 2006, 47, 2106.
23. Ginzburg, V. V. Macromolecules 2005, 38, 2362.
24. Thompson, R. B.; Ginzburg, V. V.; Matsen, M. W.; Balazs, A. C. Macromolecules 2002, 35, 1060.
25. Huh, J.; Ginzburg, V. V.; Balazs, A. C. Macromolecules 2000, 33, 8085.
26. Ginzburg, V. V.; Qiu, F.; Paniconi, M.; Peng, G.; Jasnow, D.; Balazs, A. C. Phys Rev Lett 1999, 82, 4026.
27. Thompson, R. B.; Ginzburg, V. V.; Matsen, M. W.; Balazs, A. C. Science 2001, 292, 2469.
28. Wu, G. Z.; Asai, S.; Sumita, M. Macromolecules 2002, 35, 945.
29. Nesterov, A. E.; Lipatov, Y. S. Polymer 1999, 40, 1347.
30. Lipatov, Y. S.; Nesterov, A. E.; Ignatova, T. D.; Nesterov, D. A. Polymer 2002, 43, 875.
31. Lee, J. Y.; Thompson, R. B.; Jasnow, D.; Balazs, A. C. Macromolecules 2002, 35, 4855.
32. Lee, J. Y.; Balazs, A. C.; Thompson, R. B.; Hill, R. M. Macromolecules 2004, 37, 3536.
33. Everaerta, V.; Aertsb, L.; Groeninckxa, G. Polymer 1999, 40, 6627.
34. Karim, A.; Liu, D. W.; Douglas, J. F.; Nakatani, A. I.; Amis, E. J. Polymer 2000, 41, 8455.
35. Sengupta, R.; Bandyopadhyay, A.; Sabharwal, S.; Chaki, T. K.; Bhowmick, A. K. Polymer 2005, 46, 3343.